



1 **The shifting of secondary inorganic aerosols formation mechanism**  
2 **during haze aggravation: The decisive role of aerosol liquid water**  
3

4 **Fei Xie<sup>1,2</sup>, Yue Su<sup>1,3</sup>, Yongli Tian<sup>2</sup>, Yanju Shi<sup>2</sup>, Xingjun Zhou<sup>2</sup>, Peng Wang<sup>2</sup>, Ruihong Yu<sup>1</sup>,**  
5 **Wei Wang<sup>1</sup>, Jiang He<sup>1,3</sup>, Jinyuan Xin<sup>4,\*</sup>, Changwei Lü<sup>1,3,\*</sup>**  
6

7 <sup>1</sup> School of Ecology and Environment, Inner Mongolia University, 010021, Hohhot, China

8 <sup>2</sup> Inner Mongolia Environmental Monitoring Center, 010011, Hohhot, China

9 <sup>3</sup> Institute of Environmental Geology, Inner Mongolia University, 010021, Hohhot, China

10 <sup>4</sup>State Key Laboratory of Atmospheric Boundary Layer Physics and Atmospheric Chemistry (LAPC), Institute of Atmospheric  
11 Physics, Chinese Academy of Sciences, Beijing 100029, China  
12

13 **Abstract**

14 Although many considerable efforts have been done to reveal the driving factors on haze aggravation,  
15 however, the roles of aerosol liquid water (ALW) in SIAs formation were mainly focused on the condition  
16 of aerosol liquid water content (ALWC) $<100\text{ ug/m}^3$ . Based on the in-situ high-resolution field observation,  
17 this work studied the decisive roles and the shifting of secondary inorganic aerosols formation mechanism  
18 during haze aggravation, revealing the different roles of ALWC in a broader scale ( $\sim 500\text{ ug/m}^3$ ) in nitrate  
19 and sulfate formation induced by aqueous chemistry in ammonia-rich atmosphere. The results showed that  
20 chemical domains of perturbation gas limiting the generation of secondary particulate matters presented  
21 obvious shifts from  $\text{HNO}_3$  sensitive to  $\text{HNO}_3$  and  $\text{NH}_3$  co-sensitive regime with the haze aggravation,  
22 indicating the powerful driving effects of ammonia in ammonia-rich atmosphere. When  $\text{ALWC}<75\text{ ug/m}^3$ ,  
23 the sulfate generation was preferentially triggered by the high ammonia utilization, then accelerated by  
24 nitrogen oxide oxidation from Clean to Moderate pollution stages, characterizing as  $\text{NOR}<0.3$ ,  $\text{SOR}<0.4$ ,  
25  $\text{NTR}<0.7$  and the molar ratio of  $\text{NO}_3^-:\text{SO}_4^{2-}=2:1$ . While  $\text{ALWC}>75\text{ ug/m}^3$ , aqueous-phase chemistry reaction  
26 of  $\text{SO}_2$  and  $\text{NH}_3$  in ALW became the prerequisite for SIAs formation driven by Henry's law in the ammonia-  
27 rich atmosphere during Heavy and Serious stages, characterizing as high  $\text{SOR}$  (0.5-0.9),  $\text{NOR}$  (0.3-0.5),  
28  $\text{NTR}>0.7$  and the molar ratio of  $\text{NO}_3^-:\text{SO}_4^{2-}=1:1$ . A positive feedback of sulfate on nitrate production was  
29 also observed in this work. Our results provided the evidence for the response of the transition ALWC with  
30 seasonal variability and climate change. It implies the target controlling of haze should not simply focus on  
31  $\text{SO}_2$  and  $\text{NO}_2$ , more attention should be paid on gaseous precursors (e.g.,  $\text{SO}_2$ ,  $\text{NO}_2$ ,  $\text{NH}_3$ ) and aerosol  
32 chemical constitution during different haze stages.

33 **Keywords:** Mechanism shifting, Aerosol liquid water, Secondary inorganic aerosols, Haze  
34 aggravation, In-situ observation

---

\* Corresponding author, Email: xjy@mail.iap.ac.cn; lcw2008@imu.edu.cn



## 35 **1 Introduction**

36 Atmospheric aerosol liquid water (ALW), which determined by ambient relative humidity  
37 (RH), has been proposed as a container since it could provide the reaction medium for the  
38 multiphase chemistry during the haze process (Ansari and Pandis, 2000; Shiraiwa et al., 2012;  
39 Davies and Wilson, 2015). Aerosol liquid water content (ALWC) was reported associating with  
40 the formation of secondary inorganic aerosols (SIAs), especially sulfates and nitrates, during  
41 the haze periods (Wu et al., 2018; Zheng et al., 2015a; Wang et al., 2016; Cheng et al., 2016;  
42 Carlton and Turpin, 2013; Nguyen et al., 2014; Xue et al., 2014; Tan et al., 2017; Liu et al.,  
43 2017b). Recently, the roles of ALWC on the generations of particulate sulfate generations  
44 (Wang et al., 2016; Cheng et al., 2016) and global secondary organic aerosols (Hodas et al.,  
45 2014; Mcneill, 2015; Wong et al., 2015) were reported. Thus, fully understanding ALW and its  
46 roles during haze aggravation is fundamentally important on atmospheric physicochemical  
47 processes, especially the liquid chemical transformation of SO<sub>2</sub> and NO<sub>x</sub> in ALW.

48 Ammonia is the most important alkaline gas, neutralizing with acidic species to form  
49 ammonium salts. Due to little attention has been paid to NH<sub>3</sub> emissions by Chinese government,  
50 atmospheric NH<sub>3</sub> experienced a significant increasing trend (Ge et al., 2019; Fu et al., 2017).  
51 Although the increase in atmospheric NH<sub>3</sub> is beneficial to reduce atmospheric acidity (Liu et  
52 al., 2019), its chemical behavior on regional haze formation is still debating. Cheng et al. (2016)  
53 indicated that the fast transform of gaseous SO<sub>2</sub> to particle sulfate under polluted conditions is  
54 attributed to the neutralization of NH<sub>3</sub>, which raises particle pH and thereby facilitated the  
55 aqueous oxidation of S (VI) by NO<sub>2</sub>. Fang et al. (2017) stated that NH<sub>3</sub> partition significantly  
56 modified aerosol pH and thereby adjusting the partition of SO<sub>2</sub> and NO<sub>2</sub>. Although the role of  
57 NH<sub>3</sub> has been identified from a theoretical perspective, the lack of NH<sub>3</sub> emission control sets  
58 barriers for more effective reduction of PM<sub>2.5</sub>. Therefore, it is urgent to fully understand the  
59 chemical regimes and behavior of reactive gases during different pollution stages and propose  
60 reasonable strategies.

61 So far, the SIAs formation has been extensively studied during short-term, continuous or  
62 persistent haze episodes, proposing several heterogeneous and homogeneous oxidation  
63 pathways on sulfate and nitrate formation (Guo et al., 2014; Li et al., 2017; Zheng et al., 2015b;  
64 Huang et al., 2014; Liu et al., 2021; Yao et al., 2020; Zhou et al., 2018b; Wang et al., 2019). In  
65 ammonia-rich atmosphere, NH<sub>3</sub> partition significantly modified aerosol pH, adjusted the  
66 partition of SO<sub>2</sub> and NO<sub>2</sub> (Fang et al., 2017) and promotes the aqueous oxidation of S (VI) by  
67 NO<sub>2</sub> (Wang et al., 2016; Cheng et al., 2016). Although many considerable efforts have been  
68 done to reveal the driving factors on haze aggravation, however, the roles of ALW in SIAs



69 formation were mainly focused on the condition of  $ALWC < 100 \mu\text{g}/\text{m}^3$  (Nenes et al., 2020; Wu  
70 et al., 2018; Bian et al., 2014; Jin et al., 2020). Therefore, the roles of ALWC in a broader scale  
71 and the mechanism shifting of secondary inorganic aerosols formation during haze aggravation  
72 in ammonia-rich atmosphere need to be understood in depth. Based on a continuous  
73 observation with 1-hour resolution from December 2019 to January 2020, this work will be  
74 helpful for fully understanding the shift of dominant mechanism with different ALWC levels  
75 during different pollution stages and proposing more effective  $PM_{2.5}$  control strategies for cities  
76 with significant characteristics of heating season.

77

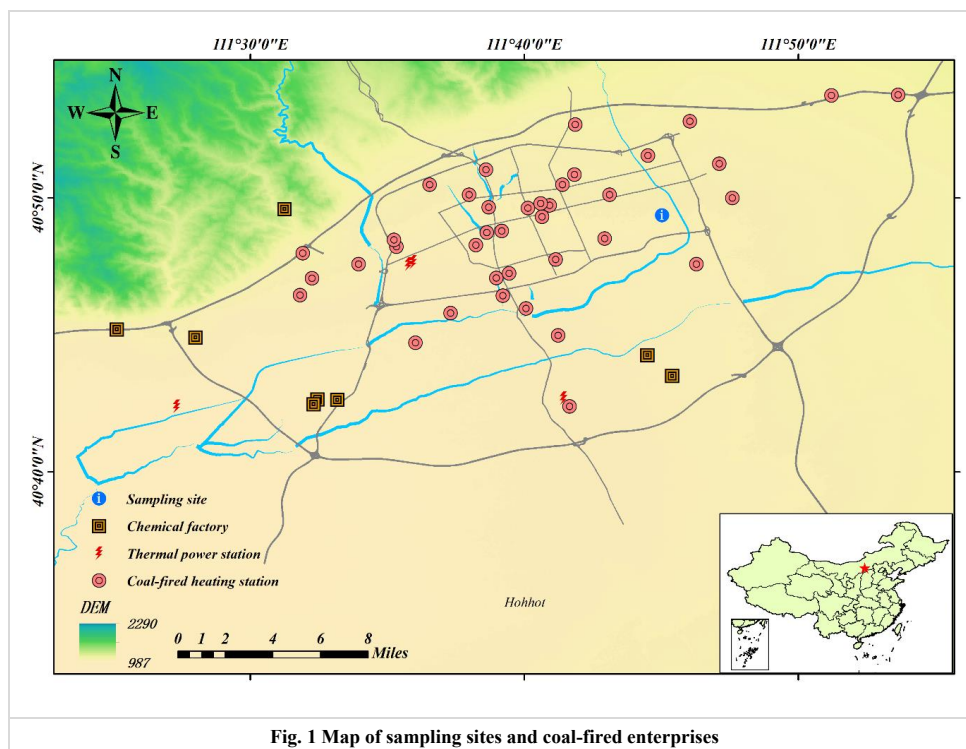
## 78 **2 Sampling and Experiment Methods**

### 79 **2.1 Description of Sampling Site**

80 Hohhot, the capital city of Inner Mongolia Autonomous Region, is the central city of Hohhot-  
81 Baotou-Ordos group, as well as an important northern China city with a population of more  
82 than 3.126 million and an area of 17224  $\text{km}^2$  (Fig. 1). This region is featured as continental  
83 climate with marked seasonality changes, which characterized as long-lasting cold humid  
84 winter and short-time other seasons. Thereby, to survive the cold season, approximately half  
85 year of coal-fired heating events (Oct. 15-the following Apr. 15) were introduced, which  
86 emitting gaseous pollutants as well as PMs around-the-clock. The main industries include  
87 thermal power plants, coal-energy based biochemical industry, dairy industry and  
88 petrochemical industry, etc., which also emit atmospheric pollutants ceaselessly. Thus, high  
89 concentrations of PMs pollution cases dominated the major contamination cases during winter  
90 season (data obtained from Department of Ecology and Environment of Inner Mongolia  
91 Autonomous Region, <http://sthjt.nmg.gov.cn/>) and gradually emerging as the limiting factor on  
92 regional ambient air quality and human health.

93 In this study, the observation was conducted at the Inner Mongolia Environmental  
94 Monitoring Center ( $40^{\circ}49'22''\text{N}$ ,  $111^{\circ}45'2''\text{E}$ ) on a top of a sixteen-story building ( $\sim 40\text{m}$  above  
95 the ground level) located at the eastern part of the downtown near the People's Government of  
96 Inner Mongolia Autonomous Region near the 2nd ring road from December 1, 2019 to January  
97 31, 2020. Residential and administrative regions were characterized as the major functional  
98 domain near the sampling site, with no direct industrial regions nearby.

99



100

## 101 **2.2 Data acquisition and analysis methods**

102 The data acquisition and analysis methods were detailed in Supplementary Material  
103 (Supplement, S1.1.1-S1.1.2) and the estimating method of aerosol pH was provided in the  
104 section of S1.1.4. The heterogeneous sulfate production was estimated as follows:

105 Due to the necessity of precise  $\text{SO}_4^{2-}$  generation, heterogeneous sulfate production ( $P_{\text{het}}$ )  
106 was parameterized and calculated according to the following equation published by Jacob  
107 (2000) and Zheng et al. (2015a).

$$108 \quad P_{\text{het}} = \frac{3600\text{sh}^{-1} \times 96\text{gmol}^{-1} \times P \left( \frac{R_p}{D_g} + \frac{4}{v\gamma} \right)^{-1}}{R \times T} S_p[\text{SO}_2(g)]$$

109 Where  $P_{\text{het}}$  was presented in  $\mu\text{g}\cdot\text{m}^{-3}\cdot\text{h}^{-1}$ ,  $3600\text{sh}^{-1}$  is time conversion factor,  $96\text{ g/mol}$  is the  
110 molar mass of  $\text{SO}_4^{2-}$ ,  $P$  is atmospheric pressure in kPa,  $R$  is the gas constant with the value of  
111  $8.31\text{ Pa}\cdot\text{m}^3\cdot\text{mol}^{-1}\cdot\text{K}^{-1}$ ,  $T$  is the temperature with the unit of K,  $R_p$  represented the radius of  
112 aerosol particles (m),  $D_g$  is the  $\text{SO}_2$  molecular diffusion coefficient and  $v$  is the mean molecular  
113 speed of  $\text{SO}_2$  with the typical tropospheric value of  $2\times 10^{-5}\text{m}^2\cdot\text{s}^{-1}$  and  $300\text{ m}\cdot\text{s}^{-1}$ , respectively.  $\gamma$   
114 is the uptake coefficient of  $\text{SO}_2$  on aerosols,  $S_p$  is the aerosol surface area per unit volume of  
115 air ( $\text{m}^2\cdot\text{m}^{-3}$ ) (Jacob, 2000).  $\text{PM}_{2.5}$  mass concentrations ( $\mu\text{g}\cdot\text{m}^{-3}$ ) and mean radius (m) during



116 campaign were roughly calculated utilizing the following empirical formula published by Guo  
117 et al. (2014):

$$118 \quad R_p = (0.254 \times C_{(PM_{2.5})} + 10.259) \times 10^{-9}$$

119 mean density of particles  $\rho$  was calculated and showed as  $1.5 \times 10^6 \text{ g}\cdot\text{m}^{-3}$  using the volume  
120 and surface area formulas of a sphere (Guo et al., 2014).  $S_p$  was estimated from the following  
121 formula:

$$122 \quad S_p = \frac{C_{(PM_{2.5})} \times 10^{-6} \text{ g} \cdot \mu\text{g}^{-1}}{4/3 \cdot \pi R_p^3 \cdot \rho} \cdot 4\pi R_p^2$$

123 relative humidity-dependent  $\gamma$  were derived according to Zheng et al. (2015a) during the  
124 campaign in this work and showed as the following formular:

$$125 \quad \gamma = \begin{cases} 2 \times 10^{-5}, & \Psi \leq 50\%, \\ 2 \times 10^{-5} + \frac{5 \times 10^{-5} - 2 \times 10^{-5}}{100 - 50\%} \times (\Psi - 50\%), & 50\% \leq \Psi \leq 100\% \end{cases}$$

126 where  $\psi$  referred to RH with the unit of %.

### 127 **3 Results and Discussion**

128 Based on National Ambient Air Quality Standards (HJ633-2012), air quality index (AQI) was  
129 introduced in this work to classify pollution levels (detailed in Supplement, S2) and discuss the  
130 characteristics of atmospheric pollutants.

#### 131 ***3.1 The observed evidence for ammonia-rich atmosphere***

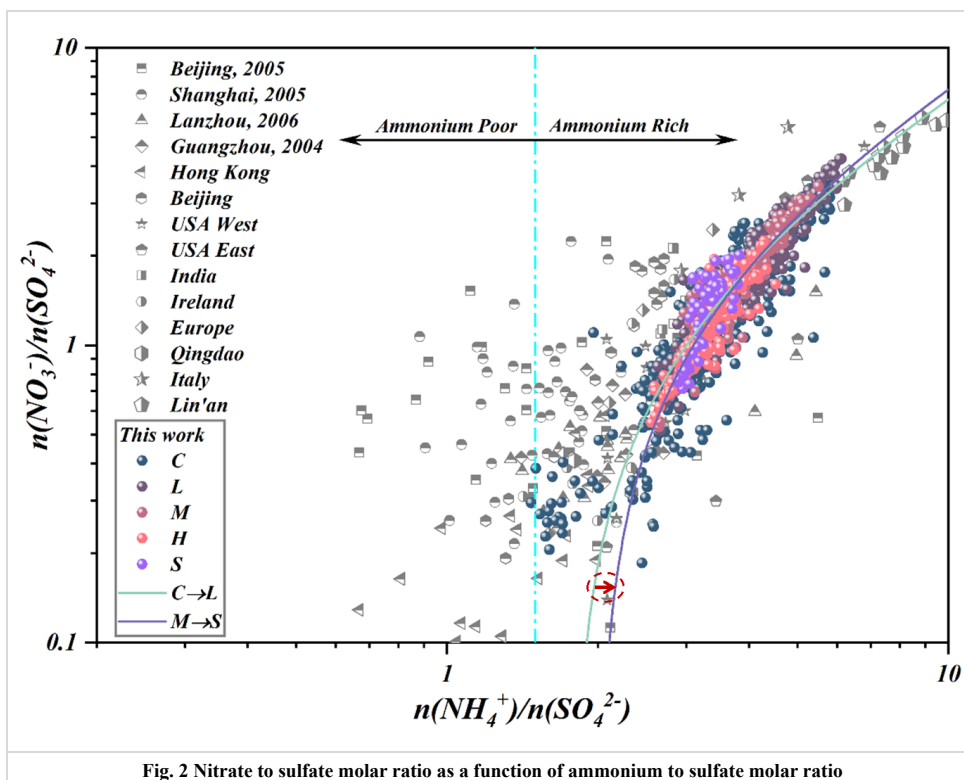
132 The characteristics of atmospheric pollutants and meteorological parameters during the studied  
133 period were summarized in Supplement (S2.1). In this work, molar ratios of  $\text{NH}_4^+$  vs. anions  
134 was used to identify the chemical species of ammonium salts (Zhou et al., 2018a; Wang et al.,  
135 2021; Liu et al., 2017b; Shi et al., 2019). The calculated results (Supplement, S2.2) showed the  
136 predominant chemical species of ammonium gradually varied from the coexistence of  
137 ammonium sulfate  $((\text{NH}_4)_2\text{SO}_4)$  and ammonium nitrate  $(\text{NH}_4\text{NO}_3)$  to the coexistence of  
138  $((\text{NH}_4)_2\text{SO}_4)$ ,  $\text{NH}_4\text{NO}_3$  and ammonium chloride  $(\text{NH}_4\text{Cl})$  with haze aggravation (Fig. S5).  
139 Further, the slope of fitted equation between excess- $\text{NH}_4^+$  and anions were still lower than 1:1  
140 line after neutralized all the measured anions, indicating the ammonia-rich atmosphere (Fig.  
141 S5c). To meet the national demand of ultra-low emissions activities (nearly two times lower  
142 than former national standard) on gaseous pollutants, heavy usage of ammonia-containing  
143 compounds in the process of desulfurization and denitrification (Solera García et al., 2017; Fu  
144 et al., 2017) at broadly distributed thermal power plants ( $>300,000\text{kWh}$ ) and the close-set coal-  
145 fired heating stations (Fig. 1) resulted ammonia fugitive provided a reasonable explanation on



146 this ammonia-rich atmosphere. Although the retrofit of national demand of ultra-low emissions  
147 activities on gaseous pollutants (nearly two times lower than former national standard) has  
148 been completed, distributed coal-based enterprises could also emit substantial SO<sub>2</sub> and NO<sub>2</sub>  
149 and subjected to heterogeneous reactions to further generate sulfate and nitrate and aggravated  
150 the haze events (Fig. S7a, S7b).

151 To show the reaction between ammonia and nitric acid and the other formation processes  
152 of nitrate in different (relative) concentrations of sulfate, the data of previous studies and  
153 different pollution levels (C, L, M, H, S) in this work were plotted in Fig. 2, indicating the  
154 characteristics of nitrate formed via the homogenous gas-phase reaction between ammonia and  
155 nitric acid. The results illustrated that the ammonia-rich regimes were not only found in Hohhot,  
156 but also observed in Guangzhou (Huang et al., 2011), Chengdu (Huang et al., 2018), Lanzhou  
157 USA West and East, India, Ireland, Europe, Qingdao, Italy, Lin'an (Pathak et al., 2009) in  
158 recent decades (Fig. 2). It suggested that atmospheric oxidative modifications driven by excess  
159 ammonia have been derived as a widespread atmospheric issue. It was worth noting that the  
160 slopes of our data were becoming steeper, coupling with the NO<sub>3</sub><sup>-</sup>/SO<sub>4</sub><sup>2-</sup> ratios change from ~4  
161 to about 1, as the increasing pollution levels. The high PM<sub>2.5</sub> nitrate concentration during Heavy  
162 and Serious stages cannot be explained by the homogeneous gas-phase reaction involving  
163 ammonia and nitric acid, which may be associating with the heterogeneous reaction in ALW  
164 on the surface of the preexisting aerosols.

165



166

### 167 **3.2 Driving mechanism of SIAs formation**

#### 168 **3.2.1 Aerosol liquid water**

169 Our results showed that SOR, NOR (the calculation detailed in Supplement, S1.1.3) and SIAs  
170 in PM<sub>2.5</sub> presented increasing trends with the increasing ALWC during the five pollution levels.  
171 The variation of predominant chemical species of ammonium (Fig. 2) indicated more SIAs will  
172 be generated on particles with the simultaneous increase of ALWC and PM<sub>2.5</sub> (Fig.3b).  
173 Theoretically, the inorganic compounds conversion was enhanced via aqueous phase chemistry  
174 on moist particles owing to the continuous partition of gaseous pollutants (e.g., SO<sub>2</sub>, NO<sub>2</sub>, N<sub>2</sub>O<sub>5</sub>)  
175 in ALWC, then disrupted the equilibrium between the gaseous and condensed phases, resulting  
176 in the aggravation of haze events (Xue et al., 2014; Wu et al., 2018; Zheng et al., 2015b; Wang  
177 et al., 2016). Considering seasonal heating characteristics, the shift of the equilibrium between  
178 gaseous and condensed phases was enhanced with the increasing atmospheric pollutants  
179 concentrations in winter due to the coal-fired combustion events. Detailly, owing to  
180 hygroscopic nature, the particles must increase their water contents via ALW along with RH  
181 (Fig. S8a) to maintain thermodynamic equilibrium and water vapor and simultaneously  
182 enhance the oxidation and dissolution of precursors in the micro-solution (ALW) of the



183 particulates. This process elevated the inorganic mass fraction as well as particulate mass  
 184 concentrations during different pollution stages (Fig. S8b) (Bertram et al., 2009; Wang et al.,  
 185 2016; Zheng et al., 2015a; Cheng et al., 2016). Due to the larger affinity of  $\text{H}_2\text{SO}_4$  for  $\text{NH}_3$  (aq),  
 186 sulfate was preferentially and fully neutralized by ammonium in the ammonia-rich atmosphere  
 187 to generate non-volatile nature of  $(\text{NH}_4)_2\text{SO}_4$  (Liu et al., 2017b; Zhou et al., 2018a; Wang et al.,  
 188 2021). Thus, SOR presented higher exponential growth with the elevated AWLC coupling with  
 189 more sulfate production (Fig. 3b). Concomitantly, the preferentially generated  $(\text{NH}_4)_2\text{SO}_4$   
 190 further enhanced the hygroscopicity of particulate matter, in turn, helped more ammonia  
 191 partitioning into moist particulate matter and generating ammonium salts accelerating haze  
 192 aggravation (Supplement, Fig. S6, Fig. S8c). Thus, most important of all, the sharp increase of  
 193 inorganic compounds associating with the elevated ALWC significantly modified the specific  
 194 surface area of particulates and further accelerated the hygroscopic aerosol growth, which  
 195 simultaneously provided a substrate for the ensuing heterogenous reaction and accelerated the  
 196 evolution of haze events. This mechanism was confirmed that the proxy of hygroscopic growth  
 197 of particulate matter ( $\text{PM}_{1.0}/\text{PM}_{2.5}$  and  $\text{PM}_{2.5}/\text{PM}_{10}$ ) gradually increased with the increasing RH,  
 198 even reaching at 95% (Fig. 3a).

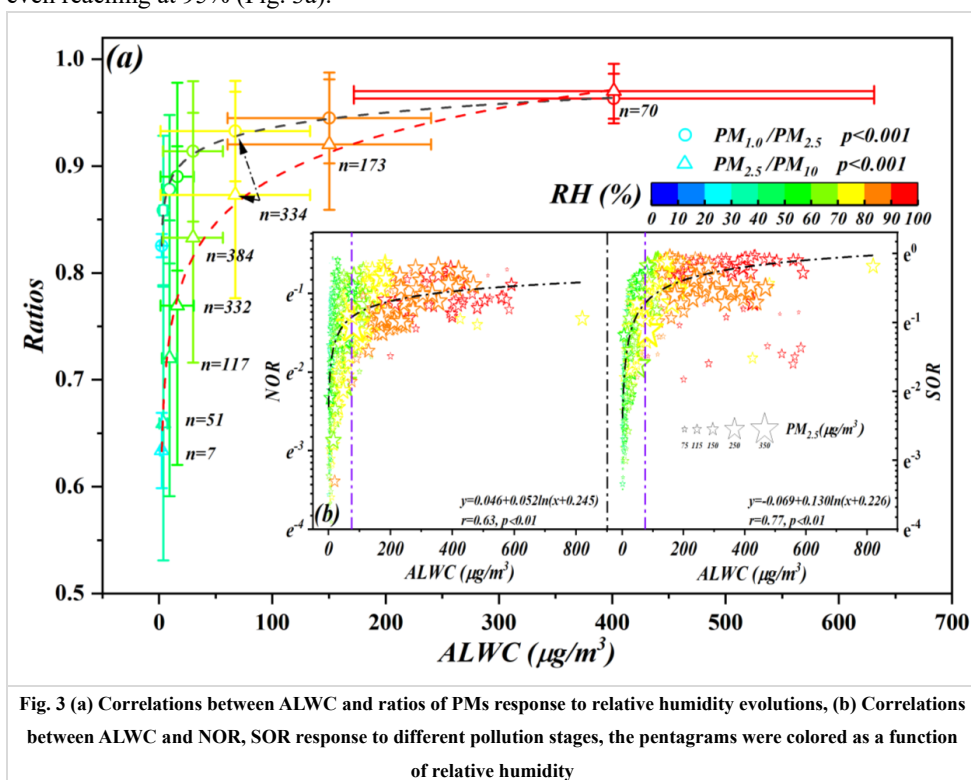


Fig. 3 (a) Correlations between ALWC and ratios of PMs response to relative humidity evolutions, (b) Correlations between ALWC and NOR, SOR response to different pollution stages, the pentagrams were colored as a function of relative humidity





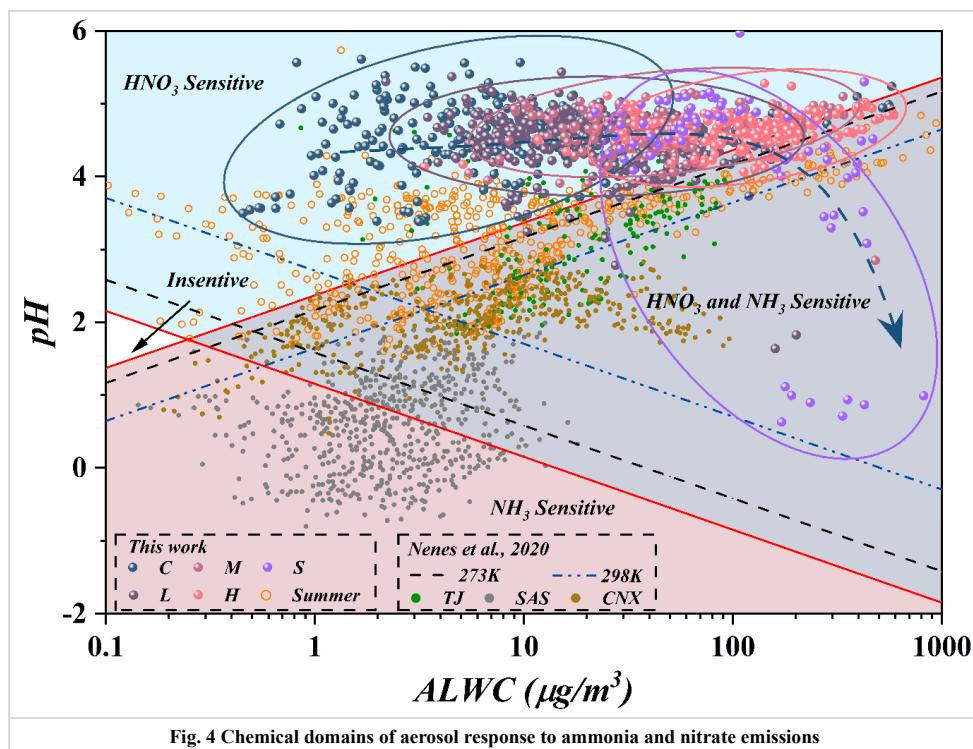
### 199 3.2.2 Perturbation gases

200 Due to the strict control of SO<sub>2</sub>, atmospheric concentrations of NO<sub>2</sub> and NH<sub>3</sub> gradually became  
201 as the decisive reactive precursors on regional atmospheric secondary particulate matter  
202 generation. Thus, the state-of-the-art framework proposed by Nenes et al. (2020) was carried  
203 out to exam the chemical domain classifications and the decisive precursor based on the data  
204 sets of previous studies (Nenes et al., 2020) and this work (Fig. 4). Due to the  
205 thermodynamically stable property of the preferentially generated (NH<sub>4</sub>)<sub>2</sub>SO<sub>4</sub>, the semi-  
206 volatile NH<sub>4</sub>NO<sub>3</sub> dominate the partitioning of NH<sub>3</sub><sup>T</sup> (sum of NH<sub>3</sub> and NH<sub>4</sub><sup>+</sup>, same to NO<sub>3</sub><sup>T</sup>)  
207 and NO<sub>3</sub><sup>T</sup>. Although aqueous NO<sub>3</sub><sup>-</sup> concentrations varied with haze processes, as an  
208 equilibrium parameter between gaseous HNO<sub>3</sub> and particle-phase NO<sub>3</sub><sup>-</sup> ( $\epsilon(\text{NO}_3^-)$ ) (Guo et al.,  
209 2016; Fang et al., 2017), the results showed the consistently full loadings of nitrate on the  
210 existing particulates during the studied period (Supplement, Fig. S9a, Fig. S9b). This could  
211 provide clear evidence for the initial HNO<sub>3</sub> sensitive area and continuous control of HNO<sub>3</sub>  
212 during the studied periods. However, with haze aggravation, significant elevated ALWC  
213 resulted in more precursors partitioned in micro-droplets to maintain water vapor. This process  
214 induced a positive shift of HNO<sub>3</sub> dissolution equilibrium and leading more HNO<sub>3</sub> partitioned  
215 on particles driven by the Henry's law (e.g., HNO<sub>3(g)</sub> ↔ HNO<sub>3(aq)</sub>,  $K_H = 2.07 \text{ mol}/(\text{L} \cdot \text{Pa})$ ). Then,  
216 the protons generated from acid dissociation in ALW activated the aqueous oxidation of the  
217 precursors to form stable acidic anions (e.g., SO<sub>4</sub><sup>2-</sup>, NO<sub>3</sub><sup>-</sup>) as well as other oxidizing agents  
218 (e.g., HONO,  $\text{NO}_2 + \text{H}_2\text{O} \xrightarrow{\text{Het}} \text{HNO}_3 + \text{HONO}$ ) (Huang et al., 2018). Meanwhile, the soluble  
219 transition metal ions, as well as OH radicals generated by HONO photolysis, also contributed  
220 to this oxidation processes (Yue et al., 2020; Zhu et al., 2020). These aqueous oxidations  
221 processes were evidenced by the observation of significantly elevated HONO and PANs during  
222 the haze aggravation (Supplement, Fig. S7c, Fig. S7d). Accordingly, the equations of  $\text{NH}_4^+ +$   
223  $\text{NO}_3^- + \text{H}^+ + \text{OH}^- \rightleftharpoons \text{NH}_4\text{NO}_3 + \text{H}_2\text{O}$  and  $\text{NH}_4^+ + \text{SO}_4^{2-} + \text{H}^+ + \text{OH}^- \rightarrow (\text{NH}_4)_2\text{SO}_4 +$   
224  $\text{H}_2\text{O}$  were shifted to generate more NH<sub>4</sub>NO<sub>3</sub> and (NH<sub>4</sub>)<sub>2</sub>SO<sub>4</sub> (Nenes et al., 2020; Gao et al.,  
225 2020) due to the driving force of more ammonia partitioned in elevated ALWC (NH<sub>3</sub>+H<sub>2</sub>O ⇌  
226 NH<sub>3</sub>·H<sub>2</sub>O, NH<sub>3</sub>·H<sub>2</sub>O ⇌ NH<sub>4</sub><sup>+</sup>+OH<sup>-</sup>). Therefore, NH<sub>3</sub> and NO<sub>x</sub> became as the decisive factors on  
227 regional atmospheric oxidability in the ammonia-rich regime (Zhai et al., 2021; Fu et al., 2017;  
228 Liu et al., 2019; Li et al., 2019).

229 Generally, both NH<sub>3</sub> and HNO<sub>3</sub> were the limiting factors governing the aerosol generations  
230 for cities of North China due to high loadings of atmospheric ammonia, while NH<sub>3</sub> governed  
231 PM formation for the southeast US (SAS) (Zhao et al., 2020). Although both cities located in  
232 US, the findings in California (CNX) were quite interesting and distributed in the insensitive

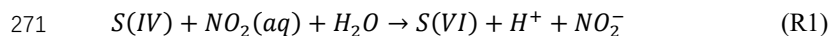


233 region and the combined  $\text{NH}_3\text{-HNO}_3$  sensitive region due to the moderate  $\text{NH}_3$  levels and the  
234 complicated atmospheric conditions during the observation (Nenes et al., 2020). In our work,  
235 the data points in summer mostly lied in  $\text{HNO}_3$  sensitive region. In winter, chemical domains  
236 of perturbation gas limiting the generation of secondary particulate matters presented obvious  
237 shifts from  $\text{HNO}_3$  sensitive to  $\text{HNO}_3$  and  $\text{NH}_3$  co-sensitive regime with the haze aggravation.  
238 Some data points of this work lied in the combined  $\text{NH}_3\text{-HNO}_3$  region in winter owing to the  
239 more acidic condition. Under the stable pH of secondary inorganic aerosols in winter at Hohhot  
240 ( $\text{pH}=4\text{-}5$ ), the more important is that a fraction of points will distribute in the combined  $\text{NH}_3\text{-}$   
241  $\text{HNO}_3$  region when  $\text{ALWC}>75 \mu\text{g}/\text{m}^3$ , which may be attributed to the liquid chemical  
242 transformation driven by Henry's law mentioned above due to the elevating ALWC.  
243 Comparatively, the pH of secondary inorganic aerosols in summer was significantly lower than  
244 those in winter in Hohhot. Compared to Tianjin, the pH of secondary inorganic aerosols in  
245 Hohhot in winter was also significant higher (Fig. 4) due to the acidity of atmospheric PM is  
246 largely depended the alkaline material in surface soils in arid and semi-arid region of China. In  
247 terms of seasonal characteristics, the higher temperature in summer elevates the volatility of  
248  $\text{NH}_4\text{NO}_3$  and dominates the partitioning of  $\text{NH}_3^{\text{T}}$  in atmospheric phase to decrease the pH of  
249 secondary inorganic aerosols. Therefore, as can be seen from Fig. 4, the data points measured  
250 in winter (Hohhot and Tianjin) characterized as higher pH and low ALWC than those in  
251 summer (Hohhot, SAS, CNX). According to the framework of Nenes et al. (2020), the  
252 transition points of Hohhot (whether winter or summer) between  $\text{NH}_3$ -dominated and  $\text{HNO}_3$ -  
253 dominated sensitivity also occurs at a pH around 2 but at lower levels of ALWC. Theoretically,  
254 it should be associated with the more aridity of Hohhot locating in the arid and semi-arid region  
255 of China. Our results provided the evidence for "the additional insight" proposed by Nenes et  
256 al. (2020) that the transition ALWC varies with season change and the aridity of sites, in  
257 response to seasonal variability and climate change. Although this effort could provide sound  
258 explanation for limiting gaseous pollutants on PM formation, mechanisms on their chemical  
259 domains, especially the roles of ALW in different locations with various conditions need further  
260 study in the future.



### 261 3.2.3 The shifting of SIAs formation mechanism driven by ALW

262 It's worth noting that two independent correlations were found between SOR and odd oxygen  
 263 ( $O_x$ ,  $O_x=NO_2+O_3$ ) during the aggravating processes of haze events, indicating the differential  
 264 mechanisms of atmospheric oxidability on sulfate generations at different stages (Fig. 5a).  
 265 Different to inefficient homogeneous sulfate oxidation efficiency (Supplement, Fig. S10),  
 266 significant correlations pairs of  $NO_2$  with SOR (Fig.5b) and NOR with  $SO_4^{2-}$  (Fig.5c) suggested  
 267 the haze aggravation was largely related to the regional  $NO_2$  levels due to the regulating effects  
 268 on atmospheric oxidizability. Thus, the aqueous-phase oxidation of S(IV) by  $NO_2$  (aq) was  
 269 triggered and accelerated by the increasing ALWC and the following equation (Yao et al., 2020;  
 270 Wang et al., 2016) (Supplement, Fig. S11a):



272 Meanwhile, sharp logarithmic increase between SOR and  $NH_4^+$  were also observed from Clean  
 273 to Moderate pollution stages (Supplement, Fig. S12). Due to the joint effects of ammonia-rich  
 274 atmosphere and ammonia's extremely water-soluble property, sufficient hydroxide generated  
 275 by ammonia dissolution forced the  $NO_2$  partitioned in ALW to maintain pH through  
 276 neutralization and producing sulfate via R1. Thus, the following equation (R2) was derived  
 277 with considering the processes of ammonia hydrolysis, which was evidenced by Fig. S11b.



278  $S(IV) + NO_2(aq) + NH_3(aq) + H_2O \rightarrow S(VI) + NH_4^+ + NO_2^- + H^+ + NO_3^-$  (R2)  
 279 Generally,  $NOR < 0.1$  means insignificant nitrogen oxide oxidation, therefore the observed  
 280 regime shift of nitrate and ammonia chemical behavior on sulfate generation suggested the  
 281 sulfate generation was preferentially triggered by the high ammonia utilization, then  
 282 accelerated by the co-effects of ammonia utilization and nitrogen oxide oxidation (Fig. 5c).

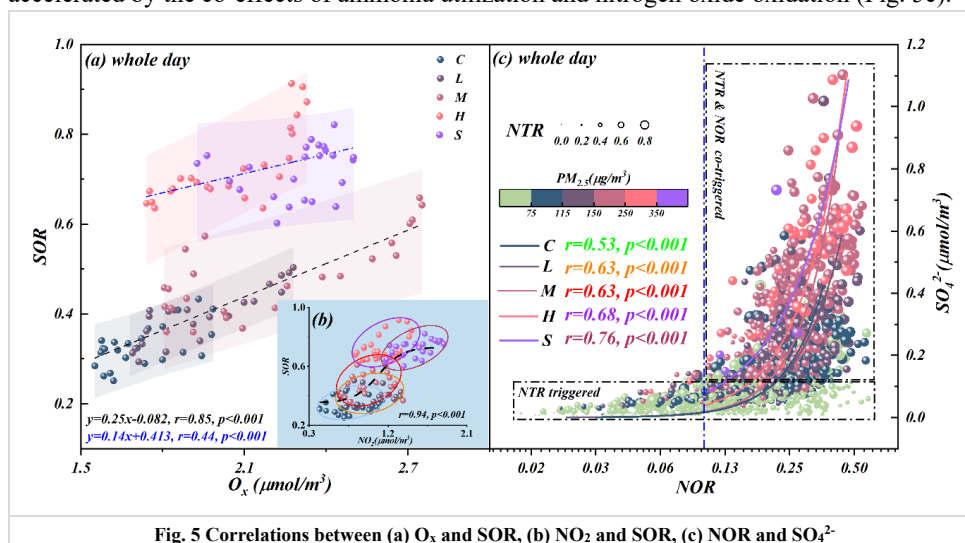


Fig. 5 Correlations between (a)  $O_3$  and SOR, (b)  $NO_2$  and SOR, (c) NOR and  $SO_4^{2-}$

283 Accordingly, the reaction R2 was activated due to the increased ALWC forced more  
 284 ammonia to partition into moist particulate matter driven by the Henry's law in the ammonia-  
 285 rich atmosphere ( $NH_3(g) \rightarrow NH_3(aq)$ ) (Supplement, Fig. S9c) (Clegg et al., 1998; Wu et al., 2018;  
 286 Gao et al., 2020). Meanwhile, our measured aqueous generated  $NO_3^-$  nicely matched theoretical  
 287 nitrate aqueous generation curve proposed by Guo et al. (2017) (Supplement, Fig. S9a, S9b),  
 288 suggesting the pathway of fast sulfate formation from oxidation of S(IV) by  $NO_2$  to generate  
 289 HONO (Wang et al., 2020) (Supplement, Fig. S11) via the reaction R2. As a result, the  
 290 thermodynamically stable  $(NH_4)_2SO_4$  would be preferentially formed to maintain its water  
 291 vapor pressure and thermodynamic equilibrium, then triggered the haze formation. Thus, the  
 292 mentioned effects resulted in a pronounced increase of  $NH_3$  partitioning with the haze  
 293 aggravation, suggesting the importance of ammonia partition on sulfate generations, namely,  
 294 NTR-controlled regime with  $ALWC < 75 \mu\text{g}/\text{m}^3$ . In summary, when  $ALWC < 75 \mu\text{g}/\text{m}^3$ , the  
 295 sulfate generation was preferentially triggered by high ammonia utilization, then accelerated  
 296 by nitrogen oxide oxidation from Clean to Light pollution stages (Fig. 5c) with  $NOR < 0.3$ ,  
 297  $SOR < 0.4$  and  $NTR < 0.7$ . In this period, the chemical composition of SIAs characterized as the  
 298 molar ratio of  $NO_3^- : SO_4^{2-} = 2:1$  (Fig. 6).

299 When  $ALWC > 75 \mu\text{g}/\text{m}^3$ , the haze was aggravated from Moderate to Serious stages along



300 with the increasing ALWC. As a result of increase in ALW, large amount of  $H^+$  was dissociated  
301 during the generation of ammonium sulfate (Supplement, Fig. S13a). From Light to Moderate  
302 pollution stages, the solubility  $SO_2$  driven by Henry's law was self-limiting due to the acidity  
303 effect in low ALWC (with  $ALWC < 75 \mu g/m^3$ ). Therefore, low sulfate concentrations coupled  
304 with low ALWC at the beginning of haze event (Supplement, Fig. S13a). However, due to the  
305 co-effects of elevated ALWC and hygroscopic nature of pre-generated ammonia sulfate,  $H^+$   
306 concentrations were diluted and nearly constant in-situ pH with the increase of ALWC during  
307 Heavy and Serious pollution stages (Supplement, Fig. S14) (Wang et al., 2016; Clifton et al.,  
308 1988; Huie and Neta, 1986; Lee and Schwartz, 1982). Hence, the significantly elevated ALWC  
309 provided more chance for the partition of  $SO_2$ ,  $NO_2$  and  $NH_3$  in ALW from Moderate to Serious  
310 pollution stages. Theoretically, Henry's constants of  $NO_2$  ( $9.74 \times 10^{-8} \text{ mol} \cdot (\text{L} \cdot \text{Pa})^{-1}$ ) is 3-4 orders  
311 of magnitude lower than those of  $SO_2$  ( $1.22 \times 10^{-5} \text{ mol} \cdot (\text{L} \cdot \text{Pa})^{-1}$ ) and  $NH_3$  ( $6.12 \times 10^{-4}$   
312  $\text{mol} \cdot (\text{L} \cdot \text{Pa})^{-1}$ ), however, it is worth noting that the aqueous generated  $NO_3^-$  from Moderate to  
313 Serious stages rapidly increased 2-5 times higher than Clean and Light stages (Supplement,  
314 Fig. S8b). Meanwhile, our monitoring results showed that the solar spectrophotometry at  
315 380nm from Moderate to Serious stages was less than 1/4 of that in clean days (Supplement,  
316 Fig. S15), suggesting the predominant of  $NO_2$  aqueous oxidation than chain photolysis (Huang  
317 et al., 2018). Accordingly, it could be deduced that aqueous-phase chemistry reaction of  $SO_2$   
318 and  $NH_3$  in ALW, driven by Henry law, became the dominant mechanism for sulfate formation  
319 due to more  $NO_2$  was required to take part in the fast sulfate formation with the increase of  
320 ALWC in the ammonia-rich atmosphere by the reaction R2. Thus, with the increasing of ALWC,  
321 high concentrations of sulfate and nitrate with high SOR (0.5-0.9), NOR (0.3-0.5) and NTR  
322 ( $>0.7$ ) induced the haze events becoming Heavy and Serious levels (Fig. 5c). Simultaneously,  
323 the calculated heterogeneous sulfate production rate (Jacob, 2000; McNeill, 2015) (Supplement,  
324 Fig. S16) presented similar trends with the impacts of ammonia on sulfate production during  
325 different pollution stages (Xue et al., 2016; Cheng et al., 2016; Liu et al., 2020). It further stated  
326 the environmental significance of the partitioning of  $SO_2$  and  $NH_3$  between gas and aqueous  
327 (ALW) phases for SIAs formation and haze aggravation. Our results provided the evidence of  
328 significant negative correlations between HONO and  $N_2O$  (Supplement, Fig. S17) from  
329 Moderate to Serious stages and positive correlations between HONO and SOR (Supplement,  
330 Fig. S11a), highlighting the recent reported secondary aqueous-phase oxidation pathway of  $SO_2$   
331 by HONO from moderate pollution period ( $2N(III) + 2S(IV) \rightarrow N_2O \uparrow + 2S(VI) +$   
332 *other products*) (Wang et al., 2020). In summary, when  $ALWC > 75 \mu g/m^3$ , aqueous-phase  
333 chemistry reaction of  $SO_2$  and  $NH_3$  in ALW became the prerequisite for SIAs formation driven



334 by Henry's law in the ammonia-rich atmosphere during Heavy and Serious stages with high  
335 SOR (0.5-0.9), NOR (0.3-0.5), NTR (>0.7). In this period, the chemical composition of SIAs  
336 characterized as the molar ratio of  $\text{NO}_3^-:\text{SO}_4^{2-}=1:1$  (Fig. 6).

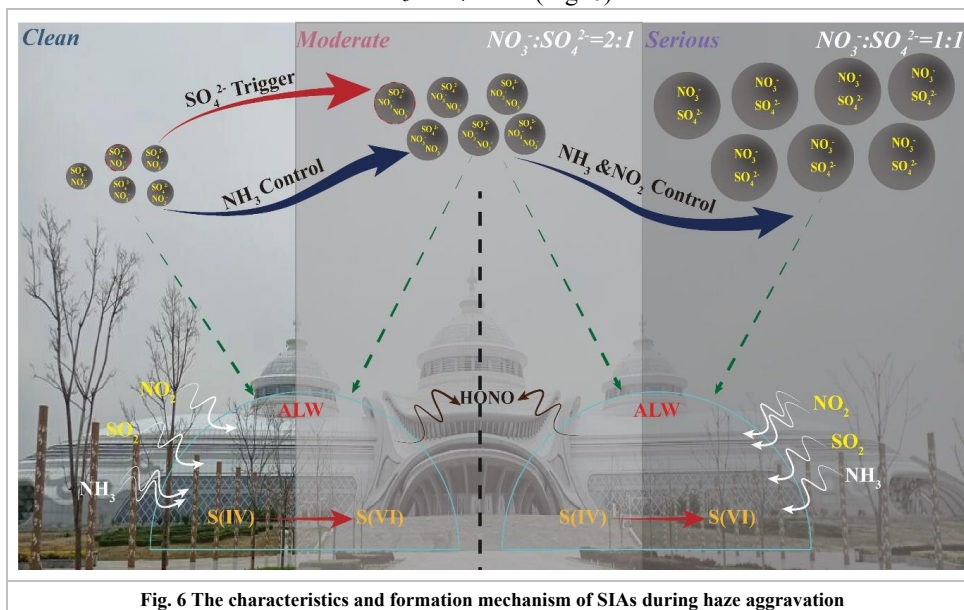
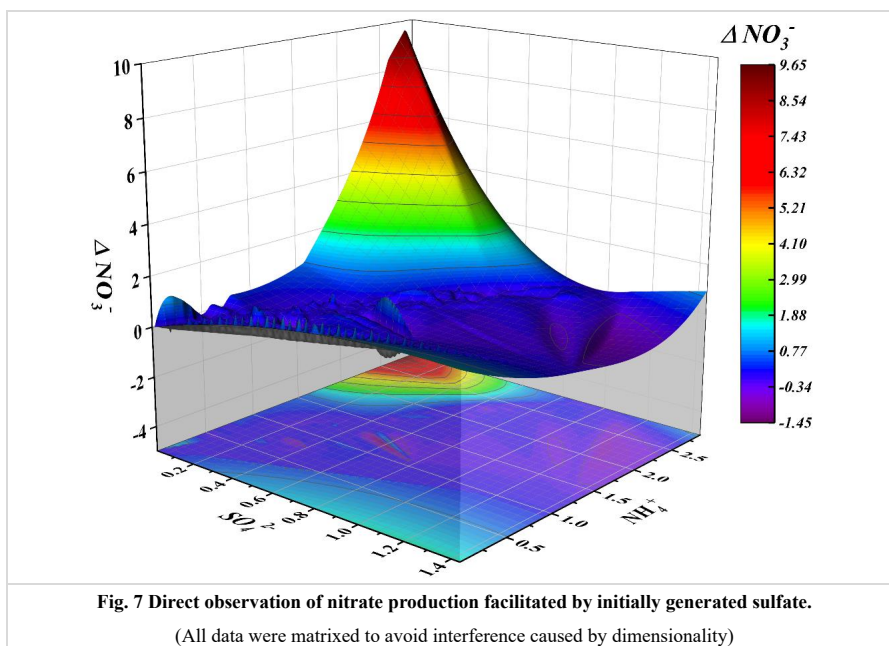


Fig. 6 The characteristics and formation mechanism of SIAs during haze aggravation

337

### 338 3.2.4 The positive feedback of sulfate on nitrate production

339 Previous works suggested that the homogeneous reaction of  $\text{NO}_2$  with OH radicals during  
340 daylight and heterogeneous hydrolysis of  $\text{N}_2\text{O}_5$  at night were the main routes on nitrate  
341 formation during haze episodes (He et al., 2018; Liu et al., 2020; Wang et al., 2019).  
342 Unsurprisingly, higher nitrate production rates ( $\Delta\text{NO}_3^-$ , the difference of hour concentrations and  
343 matrixing afterwards) were frequently observed in ammonia-rich conditions due to that  
344 ammonia-rich regime was more conducive on nitrate generation. However, the high level of  
345 nitrate production rates ( $\Delta\text{NO}_3^-$ ) were found in the area characterizing as high ammonium and  
346 low sulfate levels, suggesting that highly utilizing ammonium and pre-generated sulfate  
347 promoting particle-phase nitrate generations (Fig. 7).



348

349 Here, we proposed a hypothesis about the hydrogen ion concentration to respond the  
350 above observations. As is known to all, apart from the extremely low levels of crustal elements,  
351 ammonia is the only alkaline gas to neutralize the acidic gases in the atmosphere and generate  
352 ammonium ions (Xie et al., 2020). Thus, the concentrations of particulate sulfate and nitrate  
353 are affected by the partitioning of  $\text{NH}_4^+/\text{NH}_3$ . Thereby, higher values of  $\Delta\text{NO}_3^-$  and  $\Delta\text{SO}_4^{2-}$   
354 always occurred in the regions with higher ammonium ions were not confused (Fig. 7, Fig.  
355 S18). According to both our results and published laboratory work (Wang et al., 2016), the  
356 acidity of the particulate matter could be significantly modified by the bulk aqueous reaction  
357 between  $\text{NO}_2$  and  $\text{SO}_2$ , in which this reaction could be further enhanced due to in the presence  
358 of  $\text{NH}_3$ . As a result of the increase in RH, the partitioning of atmospheric ammonia was broken  
359 in a deep extent, which enhanced the neutralization of S(VI) by ammonia at the particle surface  
360 to generate ammonium sulfate and dissociate huge  $\text{H}^+$  (Fig. S13b, red part). Simultaneously, at  
361 the beginning of haze event, termed as relative low sulfate concentrations, the ALWC did not  
362 raised significantly (Fig. S14b). Thus, preferentially generated hydrogen ions hydrolyzed from  
363 sulfate dissociation during the early stages of contamination at low relative humidity absorb  
364 ammonia more effectively from the ammonia-rich atmosphere could promote net nitrate  
365 production significantly. However, due to the co-effects of elevated RH and hygroscopic nature  
366 of pre-generated ammonia sulfate,  $\text{H}^+$  concentrations were diluted and shown as nearly



367 constant in-situ pH (Fig. S14a). According to previous works, the reaction between firstly  
368 generated sulfate and bisulfate with ammonia were treated as the determination reaction on  
369 particle acidity (Weber et al., 2016; Liu et al., 2017a). This reaction is self-limiting due to the  
370 acidity effect, namely that it increases the acidity of aqueous phase and in turn reduces the  
371 efficiency of Henry's constant for SO<sub>2</sub> solubility and reaction rate and reduced the H<sup>+</sup> formation  
372 rates from moderate periods, compared with clean periods (Fig. S13b, blue) (Wang et al., 2016;  
373 Clifton et al., 1988; Huie and Neta, 1986; Lee and Schwartz, 1982). Due to the co-effects of  
374 RH increase and hygroscopic of sulfate, the ALWC was significantly elevated with the worsen  
375 of haze. Although more H<sup>+</sup> was generated in this process, no significant decrease in pH was  
376 found with the haze aggravation due to the dilution effect of ALWC on H<sup>+</sup>. Previous works  
377 suggested that in the case of ALWC increase, nitrate production is controlled by elevated H<sup>+</sup>  
378 associating with the increase of sulfate, namely, NO<sub>3</sub><sup>-</sup> presented elevating trend with the  
379 increases of H<sup>+</sup> concentration (Xie et al., 2020). Thus, although H<sup>+</sup> from the dissociation of  
380 sulfuric acid and full-loaded particle nitrate in conjunction with the haze aggravation generate  
381 particle HNO<sub>3</sub> (Fig. S19a) could forcing more ammonia partitioned on the particles to generate  
382 ammonium nitrate (Fig. S19b), net nitrate production ( $\Delta\text{NO}_3^-$ ) was nearly consistent.

#### 383 **4 Conclusions**

384 The formation of SIAs, especially sulfates and nitrates, was inherently associated with ALWC  
385 during the haze aggravation, in which the roles of ALWC should be more significant in  
386 ammonia-rich atmosphere. The novelty of our work is to find the shifting of secondary  
387 inorganic aerosols formation mechanism during haze aggravation and explain the different  
388 roles of ALWC in a broader scale ( $\sim 500 \text{ ug/m}^3$ ) in ammonia-rich atmosphere based on the in-  
389 situ high-resolution on-line monitoring data sets. The results showed that chemical domains of  
390 perturbation gas limiting the generation of secondary particulate matters presented obvious  
391 shifts from HNO<sub>3</sub> sensitive to HNO<sub>3</sub> and NH<sub>3</sub> co-sensitive regime with the haze aggravation,  
392 indicating the powerful driving effects of ammonia in ammonia-rich atmosphere. When  
393  $\text{ALWC} < 75 \text{ ug/m}^3$ , the sulfate generation was preferentially triggered by the high ammonia  
394 utilization, then accelerated by nitrogen oxide oxidation from Clean to Moderate pollution  
395 stages, characterizing as  $\text{NOR} < 0.3$ ,  $\text{SOR} < 0.4$ ,  $\text{NTR} < 0.7$  and the molar ratio of  $\text{NO}_3^-:\text{SO}_4^{2-}=2:1$ .  
396 While  $\text{ALWC} > 75 \text{ ug/m}^3$ , aqueous-phase chemistry reaction of SO<sub>2</sub> and NH<sub>3</sub> in ALW became  
397 the prerequisite for SIAs formation driven by Henry's law in the ammonia-rich atmosphere  
398 during Heavy and Serious stages, characterizing as high SOR (0.5-0.9), NOR (0.3-0.5), NTR  
399 ( $>0.7$ ) and the molar ratio of  $\text{NO}_3^-:\text{SO}_4^{2-}=1:1$ . A positive feedback of sulfate on nitrate  
400 production was also observed in this work. Our work provides a potential explanation for the





401 interactive mechanism and feedback between nitric aqueous chemistry and sulfate formation  
402 in ammonia-rich atmosphere based on high-resolution field observation. It implies the target  
403 controlling of haze should not simply focus on SO<sub>2</sub> and NO<sub>2</sub>, more attention should be paid on  
404 gaseous precursors (e.g., SO<sub>2</sub>, NO<sub>2</sub>, NH<sub>3</sub>) and aerosol chemical constitution during different  
405 haze stages.

406

407 *Data availability.* All data of this study are available from the corresponding author upon  
408 reasonable request (lcw2008@imu.edu.cn).

409

410 *Supplement.* The Supplement related to this article is available online at

411

412 *Author Contributions.* FX: Data curation, Formal analysis, Software, Writing-original draft.  
413 YS: Investigation, Formal analysis. YLT: Methodology, Software. YSH: Investigation, Formal  
414 analysis. XJZ: Investigation, Formal analysis, Software. PW: Methodology, Investigation.  
415 RHY: Software, Writing-review & editing. WW: Investigation, Validation, Writing-review &  
416 editing. JH: Investigation, Methodology. JYX: Investigation, Validation, Supervision, Writing-  
417 review & editing. CWL: Initiating and leading this research, Supervision, Writing-review &  
418 editing.

419

420 *Competing interest.* The authors declared that they have no conflict of interest.

421

422 *Acknowledgments.* This work is supported by Science and Technology Major Project on Air  
423 Pollution Prevention and Prediction in Hohhot-Baotou-Ordos Cities Group of Inner Mongolia  
424 (No. 2020ZD0013), National Natural Science Foundation of China (No. 42167028, 41763014)  
425 and Science Fund for Distinguished Young Scholars of Inner Mongolia (2019JQ05).

426

## 427 **References**

- 428 Ansari, A. S. and Pandis, S. N.: Water Absorption by Secondary Organic Aerosol and Its Effect on Inorganic  
429 Aerosol Behavior, *Environ. Sci. Technol.*, 34, 71-77, 10.1021/es990717q, 2000.
- 430 Bertram, T. H., Thornton, J. A., Riedel, T. P., Middlebrook, A. M., Bahreini, R., Bates, T. S., Quinn, P. K., and  
431 Coffman, D. J.: Direct observations of N<sub>2</sub>O<sub>5</sub> reactivity on ambient aerosol particles, *Geophys. Res. Lett.*, 36,  
432 <https://doi.org/10.1029/2009GL040248>, 2009.
- 433 Bian, Y. X., Zhao, C. S., Ma, N., Chen, J., and Xu, W. Y.: A study of aerosol liquid water content based on  
434 hygroscopicity measurements at high relative humidity in the North China Plain Atmos. Chem. Phys., 14,  
435 6417–6426, <https://doi.org/10.5194/acp-14-6417-2014>, 2014.
- 436 Carlton, A. and Turpin, B.: Particle partitioning potential of organic compounds is highest in the Eastern US and



- 437 driven by anthropogenic water, *Atmos. Chem. Phys.*, 13, 10203-10214, 2013.
- 438 Cheng, Y., Zheng, G., Wei, C., Mu, Q., Zheng, B., Wang, Z., Gao, M., Zhang, Q., He, K., Carmichael, G., Pöschl,  
439 U., and Su, H.: Reactive nitrogen chemistry in aerosol water as a source of sulfate during haze events in  
440 China, *Sci. Adv.*, 2, e1601530, 10.1126/sciadv.1601530, 2016.
- 441 Clegg, S. L., Brimblecombe, P., and Wexler, A. S.: Thermodynamic Model of the System  $\text{H}^+ - \text{NH}_4^+ - \text{SO}_4^{2-} - \text{NO}_3^-$   
442  $- \text{H}_2\text{O}$  at Tropospheric Temperatures, *J. Phys. Chem. A*, 102, 2137-2154, 10.1021/jp973042r, 1998.
- 443 Clifton, C. L., Altstein, N., and Huie, R. E.: Rate constant for the reaction of nitrogen dioxide with sulfur(IV) over  
444 the pH range 5.3-13, *Environ. Sci. Technol.*, 22, 586-589, 10.1021/es00170a018, 1988.
- 445 Davies, J. F. and Wilson, K. R.: Nanoscale interfacial gradients formed by the reactive uptake of OH radicals onto  
446 viscous aerosol surfaces, *Chem. Sci.*, 6, 7020-7027, 10.1039/C5SC02326B, 2015.
- 447 Fang, T., Guo, H., Zeng, L., Verma, V., Nenes, A., and Weber, R. J.: Highly Acidic Ambient Particles, Soluble  
448 Metals, and Oxidative Potential: A Link between Sulfate and Aerosol Toxicity, *Environmental Science &*  
449 *Technology*, 51, 2611-2620, 10.1021/acs.est.6b06151, 2017.
- 450 Fu, X., Wang, S., Xing, J., Zhang, X., Wang, T., and Hao, J.: Increasing Ammonia Concentrations Reduce the  
451 Effectiveness of Particle Pollution Control Achieved via SO<sub>2</sub> and NO<sub>x</sub> Emissions Reduction in East China,  
452 *Environ. Sci. Technol. Lett.*, 4, 221-227, 10.1021/acs.estlett.7b00143, 2017.
- 453 Gao, J., Wei, Y., Shi, G., Yu, H., Zhang, Z., Song, S., Wang, W., Liang, D., and Feng, Y.: Roles of RH, aerosol pH  
454 and sources in concentrations of secondary inorganic aerosols, during different pollution periods, *Atmos.*  
455 *Environ.*, 241, 117770, <https://doi.org/10.1016/j.atmosenv.2020.117770>, 2020.
- 456 Ge, B., Xu, X., Ma, Z., Pan, X., Wang, Z., Lin, W., Ouyang, B., Xu, D., Lee, J., Zheng, M., Ji, D., Sun, Y., Dong,  
457 H., Squires, F. A., Fu, P., and Wang, Z.: Role of Ammonia on the Feedback Between AWC and Inorganic  
458 Aerosol Formation During Heavy Pollution in the North China Plain, *Earth and Space Science*, 6, 1675-  
459 1693, <https://doi.org/10.1029/2019EA000799>, 2019.
- 460 Guo, H., Liu, J., Froyd, K. D., Roberts, J. M., Veres, P. R., Hayes, P. L., Jimenez, J. L., Nenes, A., and Weber, R.  
461 J.: Fine particle pH and gas-particle phase partitioning of inorganic species in Pasadena, California, during  
462 the 2010 CalNex campaign, *Atmos. Chem. Phys.*, 17, 5703-5719, 10.5194/acp-17-5703-2017, 2017.
- 463 Guo, H., Sullivan, A. P., Campuzano-Jost, P., Schroder, J. C., Lopez-Hilfiker, F. D., Dibb, J. E., Jimenez, J. L.,  
464 Thornton, J. A., Brown, S. S., Nenes, A., and Weber, R. J.: Fine particle pH and the partitioning of nitric  
465 acid during winter in the northeastern United States, *J. Geophys. Res.: Atmospheres*, 121, 10,355-310,376,  
466 <https://doi.org/10.1002/2016JD025311>, 2016.
- 467 Guo, S., Hu, M., Zamora, M. L., Peng, J., Shang, D., Zheng, J., Du, Z., Wu, Z., Shao, M., Zeng, L., Molina, M.  
468 J., and Zhang, R.: Elucidating severe urban haze formation in China, *Proc. Natl. Acad. Sci. USA*, 111,  
469 17373-17378, 10.1073/pnas.1419604111, 2014.
- 470 He, P., Xie, Z., Chi, X., Yu, X., Fan, S., Kang, H., Liu, C., and Zhan, H.: Atmospheric  $\Delta^{17}\text{O}(\text{NO}_3^-)$  reveals  
471 nocturnal chemistry dominates nitrate production in Beijing haze, *Atmos. Chem. Phys.*, 18, 14465-14476,  
472 10.5194/acp-18-14465-2018, 2018.
- 473 Hodas, N., Sullivan, A. P., Skog, K., Keutsch, F. N., Collett, J. L., Decesari, S., Facchini, M. C., Carlton, A. G.,  
474 Laaksonen, A., and Turpin, B. J.: Aerosol Liquid Water Driven by Anthropogenic Nitrate: Implications for  
475 Lifetimes of Water-Soluble Organic Gases and Potential for Secondary Organic Aerosol Formation, *Environ.*  
476 *Sci. Technol.*, 48, 11127-11136, 10.1021/es5025096, 2014.
- 477 Huang, R.-J., Zhang, Y., Bozzetti, C., Ho, K.-F., Cao, J.-J., Han, Y., Daellenbach, K. R., Slowik, J. G., Platt, S. M.,  
478 Canonaco, F., Zotter, P., Wolf, R., Pieber, S. M., Bruns, E. A., Crippa, M., Ciarelli, G., Piazzalunga, A.,  
479 Schwikowski, M., Abbazade, G., Schnelle-Kreis, J., Zimmermann, R., An, Z., Szidat, S., Baltensperger, U.,  
480 Haddad, I. E., and Prévôt, A. S. H.: High secondary aerosol contribution to particulate pollution during haze



- 481 events in China, *Nature*, 514, 218-222, 10.1038/nature13774, 2014.
- 482 Huang, X., Qiu, R., Chan, C. K., and Ravi Kant, P.: Evidence of high PM<sub>2.5</sub> strong acidity in ammonia-rich  
483 atmosphere of Guangzhou, China: Transition in pathways of ambient ammonia to form aerosol ammonium  
484 at  $[\text{NH}_4^+]/[\text{SO}_4^{2-}]=1.5$ , *Atmos. Res.*, 99, 488-495, <https://doi.org/10.1016/j.atmosres.2010.11.021>, 2011.
- 485 Huang, X., Zhang, J., Luo, B., Wang, L., Tang, G., Liu, Z., Song, H., Zhang, W., Yuan, L., and Wang, Y.: Water-  
486 soluble ions in PM<sub>2.5</sub> during spring haze and dust periods in Chengdu, China: Variations, nitrate formation  
487 and potential source areas, *Environ. Pollut.*, 243, 1740-1749, <https://doi.org/10.1016/j.envpol.2018.09.126>,  
488 2018.
- 489 Huie, R. E. and Neta, P.: Kinetics of one-electron transfer reactions involving chlorine dioxide and nitrogen  
490 dioxide, *J. Phys. Chem.*, 90, 1193-1198, 10.1021/j100278a046, 1986.
- 491 Jacob, D. J.: Heterogeneous chemistry and tropospheric ozone, *Atmos. Environ.*, 34, 2131-2159,  
492 [https://doi.org/10.1016/S1352-2310\(99\)00462-8](https://doi.org/10.1016/S1352-2310(99)00462-8), 2000.
- 493 Jin, X., Wang, Y., Li, Z., Zhang, F., Xu, W., Sun, Y., Fan, X., Chen, G., Wu, H., Ren, J., Wang, Q., and Cribb, M.:  
494 Significant contribution of organics to aerosol liquid water content in winter in Beijing, China, *Atmos. Chem.*  
495 *Phys.*, 20, 901-914, <https://doi.org/10.5194/acp-20-901-2020>, 2020.
- 496 Lee, Y. and Schwartz, S.: Kinetics of oxidation of aqueous sulfur (IV) by nitrogen dioxide, Elsevier, New York,  
497 pp 453-466 pp.1982.
- 498 Li, G., Bei, N., Cao, J., Huang, R., Wu, J., Feng, T., Wang, Y., Liu, S., Zhang, Q., Tie, X., and Molina, L. T.: A  
499 possible pathway for rapid growth of sulfate during haze days in China, *Atmos. Chem. Phys.*, 17, 3301-  
500 3316, 10.5194/acp-17-3301-2017, 2017.
- 501 Li, H., Cheng, J., Zhang, Q., Zheng, B., Zhang, Y., Zheng, G., and He, K.: Rapid transition in winter aerosol  
502 composition in Beijing from 2014 to 2017: response to clean air actions, *Atmos. Chem. Phys.*, 19, 11485-  
503 11499, 10.5194/acp-19-11485-2019, 2019.
- 504 Liu, M., Song, Y., Zhou, T., Xu, Z., Yan, C., Zheng, M., Wu, Z., Hu, M., Wu, Y., and Zhu, T.: Fine particle pH  
505 during severe haze episodes in northern China, *Geophys. Res. Lett.*, 44, 5213-5221,  
506 <https://doi.org/10.1002/2017GL073210>, 2017a.
- 507 Liu, M., Huang, X., Song, Y., Tang, J., Cao, J., Zhang, X., Zhang, Q., Wang, S., Xu, T., Kang, L., Cai, X., Zhang,  
508 H., Yang, F., Wang, H., Yu, J. Z., Lau, A. K. H., He, L., Huang, X., Duan, L., Ding, A., Xue, L., Gao, J., Liu,  
509 B., and Zhu, T.: Ammonia emission control in China would mitigate haze pollution and nitrogen deposition,  
510 but worsen acid rain, *Proc. Natl. Acad. Sci. USA*, 116, 7760-7765, 10.1073/pnas.1814880116, 2019.
- 511 Liu, P., Ye, C., Xue, C., Zhang, C., Mu, Y., and Sun, X.: Formation mechanisms of atmospheric nitrate and sulfate  
512 during the winter haze pollution periods in Beijing: gas-phase, heterogeneous and aqueous-phase chemistry,  
513 *Atmos. Chem. Phys.*, 20, 4153-4165, 10.5194/acp-20-4153-2020, 2020.
- 514 Liu, T., Chan, A. W. H., and Abbatt, J. P. D.: Multiphase Oxidation of Sulfur Dioxide in Aerosol Particles:  
515 Implications for Sulfate Formation in Polluted Environments, *Environ. Sci. Technol.*, 55, 4227-4242,  
516 10.1021/acs.est.0c06496, 2021.
- 517 Liu, Z., Xie, Y., Hu, B., Wen, T., Xin, J., Li, X., and Wang, Y.: Size-resolved aerosol water-soluble ions during the  
518 summer and winter seasons in Beijing: Formation mechanisms of secondary inorganic aerosols,  
519 *Chemosphere*, 183, 119-131, <https://doi.org/10.1016/j.chemosphere.2017.05.095>, 2017b.
- 520 McNeill, V. F.: Aqueous Organic Chemistry in the Atmosphere: Sources and Chemical Processing of Organic  
521 Aerosols, *Environ. Sci. Technol.*, 49, 1237-1244, 10.1021/es5043707, 2015.
- 522 Nenes, A., Pandis, S. N., Weber, R. J., and Russell, A.: Aerosol pH and liquid water content determine when  
523 particulate matter is sensitive to ammonia and nitrate availability, *Atmos. Chem. Phys.*, 20, 3249-3258,  
524 10.5194/acp-20-3249-2020, 2020.



- 525 Nguyen, T., Petters, M., Suda, S., Guo, H., Weber, R., and Carlton, A.: Trends in particle-phase liquid water during  
526 the Southern Oxidant and Aerosol Study, *Atmos. Chem. Phys.*, 14, 10911-10930, 2014.
- 527 Pathak, R. K., Wu, W. S., and Wang, T.: Summertime PM<sub>2.5</sub> ionic species in four major cities of China: nitrate  
528 formation in an ammonia-deficient atmosphere, *Atmos. Chem. Phys.*, 9, 1711-1722, 10.5194/acp-9-1711-  
529 2009, 2009.
- 530 Shi, G., Xu, J., Shi, X., Liu, B., Bi, X., Xiao, Z., Chen, K., Wen, J., Dong, S., Tian, Y., Feng, Y., Yu, H., Song, S.,  
531 Zhao, Q., Gao, J., and Russell, A. G.: Aerosol pH Dynamics During Haze Periods in an Urban Environment  
532 in China: Use of Detailed, Hourly, Speciated Observations to Study the Role of Ammonia Availability and  
533 Secondary Aerosol Formation and Urban Environment, *J. Geophys. Res.: Atmospheres*, 124, 9730-9742,  
534 <https://doi.org/10.1029/2018JD029976>, 2019.
- 535 Shiraiwa, M., Pfrang, C., Koop, T., and Pöschl, U.: Kinetic multi-layer model of gas-particle interactions in  
536 aerosols and clouds (KM-GAP): linking condensation, evaporation and chemical reactions of organics,  
537 oxidants and water, *Atmos. Chem. Phys.*, 12, 2777-2794, 10.5194/acp-12-2777-2012, 2012.
- 538 Solera García, M. A., Timmis, R. J., Van Dijk, N., Whyatt, J. D., Leith, I. D., Leeson, S. R., Braban, C. F., Sheppard,  
539 L. J., Sutton, M. A., and Tang, Y. S.: Directional passive ambient air monitoring of ammonia for fugitive  
540 source attribution; a field trial with wind tunnel characteristics, *Atmos. Environ.*, 167, 576-585,  
541 <https://doi.org/10.1016/j.atmosenv.2017.07.043>, 2017.
- 542 Tan, H., Cai, M., Fan, Q., Liu, L., Li, F., Chan, P., Deng, X., and Wu, D.: An analysis of aerosol liquid water  
543 content and related impact factors in Pearl River Delta, *Sci. Total Environ.*, 579, 1822-1830, 2017.
- 544 Wang, G., Zhang, R., Gomez, M. E., Yang, L., Zamora, M. L., Hu, M., Lin, Y., Peng, J., Guo, S., and Meng, J.:  
545 Persistent sulfate formation from London Fog to Chinese haze, *Proc. Natl. Acad. Sci. USA*, 113, 13630-  
546 13635, 2016.
- 547 Wang, H., Wang, X., Zhou, H., Ma, H., Xie, F., Zhou, X., Fan, Q., Lü, C., and He, J.: Stoichiometric characteristics  
548 and economic implications of water-soluble ions in PM<sub>2.5</sub> from a resource-dependent city, *Environ. Res.*,  
549 193, 110522, <https://doi.org/10.1016/j.envres.2020.110522>, 2021.
- 550 Wang, J., Li, J., Ye, J., Zhao, J., and Jacob, D. J.: Fast sulfate formation from oxidation of SO<sub>2</sub> by NO<sub>2</sub> and HONO  
551 observed in Beijing haze, *Nature Communications*, 11, 2844, 2020.
- 552 Wang, S., Yin, S., Zhang, R., Yang, L., Zhao, Q., Zhang, L., Yan, Q., Jiang, N., and Tang, X.: Insight into the  
553 formation of secondary inorganic aerosol based on high-time-resolution data during haze episodes and  
554 snowfall periods in Zhengzhou, China, *Sci. Total Environ.*, 660, 47-56,  
555 <https://doi.org/10.1016/j.scitotenv.2018.12.465>, 2019.
- 556 Weber, R. J., Guo, H., Russell, A. G., and Nenes, A.: High aerosol acidity despite declining atmospheric sulfate  
557 concentrations over the past 15 years, *Nat. Geosci.*, 9, 282-285, 10.1038/ngeo2665, 2016.
- 558 Wong, J. P. S., Lee, A. K. Y., and Abbatt, J. P. D.: Impacts of Sulfate Seed Acidity and Water Content on Isoprene  
559 Secondary Organic Aerosol Formation, *Environ. Sci. Technol.*, 49, 13215-13221, 10.1021/acs.est.5b02686,  
560 2015.
- 561 Wu, Z., Wang, Y., Tan, T., Zhu, Y., Li, M., Shang, D., Wang, H., Lu, K., Guo, S., Zeng, L., and Zhang, Y.: Aerosol  
562 Liquid Water Driven by Anthropogenic Inorganic Salts: Implying Its Key Role in Haze Formation over the  
563 North China Plain, *Environ. Sci. Technol. Lett.*, 5, 160-166, 10.1021/acs.estlett.8b00021, 2018.
- 564 Xie, Y., Wang, G., Wang, X., Chen, J., Chen, Y., Tang, G., Wang, L., Ge, S., Xue, G., Wang, Y., and Gao, J.:  
565 Nitrate-dominated PM<sub>2.5</sub> and elevation of particle pH observed in urban Beijing during the winter of 2017,  
566 *Atmos. Chem. Phys.*, 20, 5019-5033, 10.5194/acp-20-5019-2020, 2020.
- 567 Xue, J., Griffith, S. M., Yu, X., Lau, A. K. H., and Yu, J. Z.: Effect of nitrate and sulfate relative abundance in  
568 PM<sub>2.5</sub> on liquid water content explored through half-hourly observations of inorganic soluble aerosols at a



- 569 polluted receptor site, *Atmos. Environ.*, 99, 24-31, <https://doi.org/10.1016/j.atmosenv.2014.09.049>, 2014.
- 570 Xue, J., Yuan, Z., Griffith, S. M., Yu, X., Lau, A. K. H., and Yu, J. Z.: Sulfate Formation Enhanced by a Cocktail  
571 of High NO<sub>x</sub>, SO<sub>2</sub>, Particulate Matter, and Droplet pH during Haze-Fog Events in Megacities in China: An  
572 Observation-Based Modeling Investigation, *Environ. Sci. Technol.*, 50, 7325-7334,  
573 10.1021/acs.est.6b00768, 2016.
- 574 Yao, L., Fan, X., Yan, C., Kurtén, T., Daellenbach, K. R., Li, C., Wang, Y., Guo, Y., Dada, L., Rissanen, M. P., Cai,  
575 J., Tham, Y. J., Zha, Q., Zhang, S., Du, W., Yu, M., Zheng, F., Zhou, Y., Kontkanen, J., Chan, T., Shen, J.,  
576 Kujansuu, J. T., Kangasluoma, J., Jiang, J., Wang, L., Worsnop, D. R., Petäjä, T., Kerminen, V.-M., Liu, Y.,  
577 Chu, B., He, H., Kulmala, M., and Bianchi, F.: Unprecedented Ambient Sulfur Trioxide (SO<sub>3</sub>) Detection:  
578 Possible Formation Mechanism and Atmospheric Implications, *Environ. Sci. Technol. Lett.*, 7, 809-818,  
579 10.1021/acs.estlett.0c00615, 2020.
- 580 Yue, F., He, P., Chi, X., Wang, L., Yu, X., Zhang, P., and Xie, Z.: Characteristics and major influencing factors of  
581 sulfate production via heterogeneous transition-metal-catalyzed oxidation during haze evolution in China,  
582 *Atmos. Pollut. Res.*, 11, 1351-1358, <https://doi.org/10.1016/j.apr.2020.05.014>, 2020.
- 583 Zhai, S., Jacob, D. J., Wang, X., Liu, Z., Wen, T., Shah, V., Li, K., Moch, J. M., Bates, K. H., Song, S., Shen, L.,  
584 Zhang, Y., Luo, G., Yu, F., Sun, Y., Wang, L., Qi, M., Tao, J., Gui, K., Xu, H., Zhang, Q., Zhao, T., Wang,  
585 Y., Lee, H. C., Choi, H., and Liao, H.: Control of particulate nitrate air pollution in China, *Nat. Geosci.*,  
586 10.1038/s41561-021-00726-z, 2021.
- 587 Zhao, Q., Nenes, A., Yu, H., Song, S., Xiao, Z., Chen, K., Shi, G., Feng, Y., and Russell, A. G.: Using High-  
588 Temporal-Resolution Ambient Data to Investigate Gas-Particle Partitioning of Ammonium over Different  
589 Seasons, *Environ. Sci. Technol.*, 54, 9834-9843, 10.1021/acs.est.9b07302, 2020.
- 590 Zheng, B., Zhang, Q., Zhang, Y., He, K., Wang, K., Zheng, G., Duan, F., Ma, Y., and Kimoto, T.: Heterogeneous  
591 chemistry: a mechanism missing in current models to explain secondary inorganic aerosol formation during  
592 the January 2013 haze episode in North China, *Atmos. Chem. Phys.*, 15, 2031-2049, 2015a.
- 593 Zheng, G. J., Duan, F. K., Su, H., Ma, Y. L., Cheng, Y., Zheng, B., Zhang, Q., Huang, T., Kimoto, T., Chang, D.,  
594 Pöschl, U., Cheng, Y. F., and He, K. B.: Exploring the severe winter haze in Beijing: the impact of synoptic  
595 weather, regional transport and heterogeneous reactions, *Atmos. Chem. Phys.*, 15, 2969-2983, 2015b.
- 596 Zhou, H., Lü, C., He, J., Gao, M., Zhao, B., Ren, L., Zhang, L., Fan, Q., Liu, T., He, Z., Dudagula, Zhou, B., Liu,  
597 H., and Zhang, Y.: Stoichiometry of water-soluble ions in PM<sub>2.5</sub>: Application in source apportionment for a  
598 typical industrial city in semi-arid region, Northwest China, *Atmos. Res.*, 204, 149-160,  
599 <https://doi.org/10.1016/j.atmosres.2018.01.017>, 2018a.
- 600 Zhou, H., Lü, C., He, J., Gao, M., Zhao, B., Ren, L., Zhang, L., Fan, Q., Liu, T., He, Z., Dudagula, Zhou, B., Liu,  
601 H., and Zhang, Y.: Stoichiometry of water-soluble ions in PM<sub>2.5</sub>: Application in source apportionment for a  
602 typical industrial city in semi-arid region, Northwest China, *Atmospheric Research*, 204, 149-160,  
603 <https://doi.org/10.1016/j.atmosres.2018.01.017>, 2018b.
- 604 Zhu, Y., Li, W., Lin, Q., Yuan, Q., Liu, L., Zhang, J., Zhang, Y., Shao, L., Niu, H., Yang, S., and Shi, Z.: Iron  
605 solubility in fine particles associated with secondary acidic aerosols in east China, *Environ. Pollut.*, 264,  
606 114769, <https://doi.org/10.1016/j.envpol.2020.114769>, 2020.

607